

Degenerate four-wave mixing in triply-resonant Kerr cavities

David Ramirez,¹ Alejandro W. Rodriguez,^{2,3} Hila Hashemi,²
J. D. Joannopoulos,¹ Marin Soljačić,¹ and Steven G. Johnson²

¹*Department of Physics, Massachusetts Institute of Technology, Cambridge, MA 02139*

²*Department of Mathematics, Massachusetts Institute of Technology, Cambridge, MA 02139*

³*School of Science and Engineering, Harvard University, Cambridge, MA 02139*

We demonstrate theoretical conditions for highly-efficient degenerate four-wave mixing in triply-resonant nonlinear (Kerr) cavities. We employ a general and accurate temporal coupled-mode analysis in which the interaction of light in arbitrary microcavities is expressed in terms a set of coupling coefficients that we rigorously derive from the full Maxwell equations. Using the coupled-mode theory, we show that light consisting of an input signal of frequency $\omega_0 - \Delta\omega$ can, in the presence of pump light at ω_0 , be converted with quantum-limited efficiency into an output shifted signal of frequency $\omega_0 + \Delta\omega$, and we derive expressions for the critical input powers at which this occurs. We find that critical powers in the order of 10mW assuming very conservative cavity parameters (modal volumes ~ 10 cubic wavelengths and quality factors ~ 1000). The standard Manley-Rowe efficiency limits are obtained from the solution of the classical coupled-mode equations, although we also derive them from simple photon-counting “quantum” arguments. Finally, using a linear stability analysis, we demonstrate that maximal conversion efficiency can be retained even in the presence of self- and cross-phase modulation effects that generally act to disrupt the resonance condition.

PACS numbers: 42.65.Ky, 42.60.Da, 42.65.Sf, 42.65.Jx

I. INTRODUCTION

For many years, researchers have used confinement of light for a long time in a small volume (resonant cavities) to enhance light-matter interactions such as optical nonlinearities, recently entering the integrated-optics regime of smaller and smaller cavities with limited sets of interacting modes. In such systems, careful design is required to maximize the efficiency and minimize the power of a given nonlinear process such as frequency conversion [1–17], and the use of cavities can also lead to qualitatively new phenomena such as bi/multistability [1, 3, 18–31]. While the use of cavities is known to enhance nonlinear effects, every distinct nonlinear process requires a new analysis. In this paper, we consider the problem of intra-cavity degenerate four-wave mixing (DFWM): an electromagnetic cavity resonant at three frequencies ω_0 and $\omega_0 \pm \Delta\omega$, in which a third-order ($\chi^{(3)}$) nonlinearity converts an input *signal* at $\omega_0 - \Delta\omega$ to an output *shifted signal* at $\omega_0 + \Delta\omega$ in the presence of an input *pump* at ω_0 . The small- $\Delta\omega$ regime corresponds, for example, to conversion between different channels in wavelength-division multiplexing (WDM), similar to recent experimental studies of nonlinear frequency conversion in cavities [32–40]; it allows one to exploit structures like ring resonators [3] or photonic-crystal cavities [41] that support closely spaced resonances, and in Sec. IV A we show that this regime supports stable quantum-limited conversion at low signal powers for a critical pump power. Conversely, we show that the $\Delta\omega > \omega_0$ regime generalizes our previous work on intra-cavity third-harmonic generation (THG) [1, 2], and in Sec. IV B we show that this regime supports stable conversion with 100% efficiency at a critical pump and signal power. For exam-

ple, with a typical nonlinear material such as gallium arsenide (GaAs) and reasonable cavity parameters (volume ~ 10 cubic wavelengths and quality factors ~ 1000), we obtain critical powers in the milliwatts (on the order of 10mW) for both $\Delta\omega$ regimes. The standard Manley-Rowe efficiency limits are considered from both a simple photon-counting “quantum” argument [42, 43] and are also derived from purely classical coupled-mode equations [44, 45] (Sec. III), where the latter also yield stability information, critical powers, and other dynamics (Secs. IV A and IV B). The coupling coefficients in these equations are derived explicitly from the full Maxwell equations for arbitrary microcavities (Sec. II). We also show that the nonlinear dynamics lead to additional phenomena, such as multistability and limit-cycle (self-pulsing) solutions, similar to phenomena that were previously shown for other nonlinear systems [1, 18, 46, 47] (Secs. IV A and IV B). Finally, in Sec. IV C, we consider the effects of self- and cross-phase modulation (SPM and XPM), which induce nonlinear shifts in the cavity frequencies: these must be compensated by pre-shifting the resonances and also affect the stability analysis (as we previously found for THG [1]).

Although nonlinear effects in electromagnetism are weak, it is well known that confining light in a small volume and/or for a long time, as in a waveguide or cavity, can both enhance the strength and modify the nature of nonlinear phenomena [48, 49]. Much previous work in nonlinear frequency conversion has studied $\chi^{(2)}$ processes (where there is a change in the susceptibility that is proportional to the square of the electric field) such as second harmonic generation (SHG) [2, 4, 17, 46, 50–59], difference-frequency generation (DFG) [5, 6, 60–62], and optical parametric amplification (OPA) [63–65]. Stud-

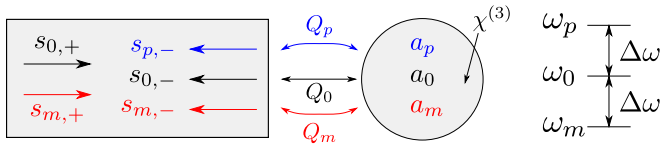


FIG. 1: (Color online) (Left) Schematic for *degenerate* four-wave mixing involving a coupled waveguide-cavity system. Dynamical variables for coupled-mode equations represent: a single input (output) channel (with incoming/outgoing field amplitudes s_{\pm}) coupled to a resonant cavity with three modes at frequencies ω_0 , $\omega_m = \omega_0 - \Delta\omega$ and $\omega_p = \omega_0 + \Delta\omega$ (and corresponding amplitudes a_0 , a_m and a_p). The three resonant modes are nonlinearly coupled by a Kerr ($\chi^{(3)}$) nonlinearity. (Right) Diagram illustrating the relationship between the three resonant frequencies.

ies of SHG in doubly resonant $\chi^{(2)}$ cavities have demonstrated that 100% conversion efficiency is achieved at critical pump power, much lower than for SHG in singly resonant cavities [2, 4, 17, 51–56, 58, 66–68]. Recent studies of DFG in triply resonant $\chi^{(2)}$ cavities also showed the existence of a critical relationship between pump and idler power that results in optimal quantum-limited conversion [60], with potential applications to terahertz generation [7, 8]. The existence of quantum-limited frequency conversion can be predicted from the Manley-Rowe relations, which govern the rates of energy transfer in nonlinear systems [48]. There has also been some recent work on intra-cavity $\chi^{(3)}$ third harmonic generation [1]. (In a $\chi^{(3)}$ medium, there is a change in the refractive index proportional to the square of the electric field.) As in SHG, THG in doubly resonant cavities has been shown to support solutions with 100% conversion efficiency, even when taking into account nonlinear frequency-shifting due to SPM and XPM, as well as interesting dynamical behavior such as multistability and limit cycles (self-pulsing) [1], with lower power requirements compared to singly resonant cavities or nonresonant structures [9, 50, 59, 65, 69, 69–81]. Limit cycles have been observed in a number of other nonlinear optical systems, including doubly resonant $\chi^{(2)}$ cavities [46, 82], bistable multimode Kerr cavities with time-delayed nonlinearities [83], nonresonant distributed feedback in Bragg gratings [19], and a number of nonlinear lasing devices [84].

In what follows, we extend the previous work on SHG, DFG and THG in resonant cavities to the case of DFWM in $\chi^{(3)}$ media. Four-wave mixing is characterized by taking input light at frequencies ω_1, ω_2 , and ω_3 and producing light at frequency $\omega_4 = \pm\omega_1 \pm \omega_2 \pm \omega_3$; degenerate four-wave mixing, however, is restricted to the case where $\omega_1 = \omega_3$ to generate $2\omega_1 - \omega_2$. Previous work has studied FWM in the context of optical fibers [85–89] and even matter waves [90], as well as demonstrating the use of FWM in applications such as phase conjugation [64, 91–93] and generation of two-photon coherent states [85, 94, 95]. While there has been recent exper-

imental work on intra-cavity FWM in $\chi^{(3)}$ media (degenerate or otherwise) [32–40, 96–98], we are not aware of any detailed studies of the underlying theoretical phenomena in general cavities. As we shall, see DFWM in triply-resonant cavities shares many qualitative features with SHG, DFG, and THG, including the existence of critical powers at which optimal conversion efficiency is achieved as well as interesting nonlinear phenomena such as limit cycles and multistability. As in DFG, and unlike SHG or THG, there exist Manley-Rowe limitations on the overall conversion efficiency. In Sec. III, we discuss the corresponding relations governing four-wave mixing and illustrate their implications for conversion efficiency. These relations can be obtained classically through temporal coupled-mode theory [44, 45], but they are more easily motivated and understood from a quantum perspective [42, 43]. Such arguments have been employed before in the context of lasing [99, 100], RF circuits [101], and other nonlinear optics phenomena [48]. In the case of intra-cavity frequency conversion, we show how both perspectives yield limits on conversion efficiency.

Several different approaches can be used to study nonlinear optical systems. Most directly, brute-force numerical simulations by a variety of methods, such as finite-difference time-domain (FDTD) [41, 102], offer the most general and flexible technique, in that they can characterize phenomena involving many degrees of freedom and going beyond the perturbative regime, but such simulations are relatively slow and allow one to study only a single geometry and excitation at a time. More abstract analyses are possible in many problems because confinement to a waveguide or cavity limits the degrees of freedom to the amplitudes of a small set of normal modes, combined with the fact that optical nonlinearities are typically weak (so that they can be treated as small perturbations to the linear modes). For example, many nonlinear phenomena have been studied in the context of co-propagating plane waves, in which the amplitudes of the waves can be shown to satisfy a set of simple ordinary differential equations (ODEs) in space (the slowly varying envelope approximation) [48]. More generally, however, it can be shown that *all* nonlinear problems coupling a finite set of modes and satisfying certain fundamental principles such as conservation of energy, regardless of the underlying wave equation (e.g. electromagnetic or acoustic waves), can be described by a *universal* set of ODEs characterized by a small number of coefficients, determined by the specific geometry and physics. This approach, which has come to be known as temporal coupled-mode theory (TCMT), dates back several decades [44, 103] and has been applied to a large number of problems, from microwave transmission systems [101] to the nonlinear intra-cavity problems (SHG, DFG, and THG) mentioned above [1, 2, 60, 103]. Likewise, we employ TCMT in this paper to characterize the most general possible behavior of intra-cavity DFWM systems, regardless of the nature of the cavity. As reviewed elsewhere [44], TCMT begins with the purely lin-

ear system and breaks it into abstract components such as input/output channels (e.g. waveguides or external losses) and cavities, characterized by resonant frequencies and coupling rates that depend on the geometry; it then turns out that the ODEs describing such a system are completely determined by those parameters once the constraints of conservation of energy, linearity, time-invariance, and reciprocity (or time-reversal invariance) are included, under the key assumption that coupling rates are slow compared to the frequencies (i.e., strong confinement) [41, 44]. Nonlinearities can then be introduced as additional terms in these equations, without disturbing the previously derived relationships, as long as the nonlinear processes are also weak (i.e. nonlinear effects occur slowly compared to the frequency), which is true in nonlinear optics [48]. Using these ODEs, the general possible behaviors can be obtained (including the Manley-Rowe relations mentioned above), but to obtain the specific characteristics of a particular geometry one then needs a separate calculation to obtain the cavity parameters. Properties of the linear modes such as frequencies and lifetimes (Q) can be obtained by standard computational methods [41, 44]. It turns out that the nonlinear coefficients can also be obtained from the linear calculations, thanks to the fact that the nonlinearities are weak: using perturbation theory, expressions for the nonlinear coefficients as integrals of the linear modes can be derived from Maxwell's equations. Such expressions were previously derived for SHG and THG [2], and also recently for DFG [60]. Here, we derive both the abstract TCMT equations and the specific nonlinear coupling coefficients for DFWM in the Maxwell equations with $\chi^{(3)}$ nonlinearities.

We begin apply the coupled-mode formalism to the case of DFWM in a triply-resonant cavity in Sec. II, to obtain the coupled-mode equations of motion as well as explicit expressions for the nonlinear coupling coefficients. We then briefly discuss general properties of the conversion process in Sec. III and, using the standard Manley-Rowe relations and simple photon-counting arguments, obtain limits on the maximal efficiency of the system. In Secs. IV A and IV B, we analyze the stability and dynamics of the solutions to the coupled-mode equations obtained in Sec. II, neglecting SPM and XPM effects, and demonstrate the existence of the maximal conversion efficiencies obtained in Sec. III. Finally, in Sec. IV C, we briefly consider the effects of SPM and XPM using a simple model to illustrate the qualitative behavior of the system; in particular, we demonstrate the existence of stable, maximal efficiency solutions even including SPM and XPM effects.

II. TEMPORAL COUPLED-MODE THEORY

We consider the situation depicted schematically in Fig. 1: an input/output channel coupled to a triply-resonant nonlinear ($\chi^{(3)}$) cavity. Here, input light at

ω_0 and $\omega_m = \omega_0 - \Delta\omega$ is converted to output light at a different frequency $\omega_p = \omega_0 + \Delta\omega$, where $\Delta\omega$ determines the separation between the three frequencies. The frequency-conversion process occurs inside the nonlinear cavity, which supports resonant modes of frequencies ω_0 , ω_m , and ω_p , and corresponding modal lifetimes τ_k (or quality factors $Q_k = \omega_k \tau_k / 2$ [44]) describing the overall decay rate ($1/\tau_k$) of the modes. In particular, the total decay rate consists of decay into the output channel, with rate $1/\tau_{s,k}$, as well as external losses (e.g. absorption) with rate $1/\tau_{e,k}$, so that $1/\tau_k = 1/\tau_{s,k} + 1/\tau_{e,k}$. Note that, to compensate for the effects of SPM/XPM, as described in [1] and in Sec. IV C, we will eventually use slightly different cavity frequencies ω_k^{cav} that have been pre-shifted away from ω_k .

It is most convenient to express the TCMT equations in terms of the following degrees of freedom [41, 44]: we let a_k denote the time-dependent complex amplitude of the k th mode, normalized so that $|a_k|^2$ is the electromagnetic energy stored in this mode, and $s_{k,\pm}$ denote the time-dependent amplitude of the incoming (+) and outgoing (−) wave, normalized so that $|s_{k,\pm}|^2$ is the power in the k th mode. (In what follows, we take $s_{p,+} = 0$, corresponding to the up-conversion of light at ω_0 and ω_m to light at ω_p , for $\Delta\omega > 0$. In order to study the alternative down-conversion process, one has but to set $\Delta\omega < 0$, in which case we effectively have $\omega_p \rightarrow \omega_m$, as described below.)

The derivation of the linear TCMT equations, corresponding to de-coupled modes a_k , has been given elsewhere [44], and the generalization to include nonlinearities has been laid out in Ref. 2. Here we introduce cubic nonlinearities and make the rotating-wave approximation (only terms with frequencies near ω_k are included in the equation of motion for a_k) [2]. This yields the following general coupled-mode equations:

$$\frac{da_0}{dt} = \left[i\omega_0(1 - \alpha_{00}|a_0|^2 - \alpha_{0m}|a_m|^2 - \alpha_{0p}|a_p|^2) - \frac{1}{\tau_0} \right] a_0 - i\omega_0\beta_0 a_0^* a_m a_p + \sqrt{\frac{2}{\tau_{s,0}}} s_{0,+} \quad (1)$$

$$\frac{da_m}{dt} = \left[i\omega_m(1 - \alpha_{m0}|a_0|^2 - \alpha_{mm}|a_m|^2 - \alpha_{mp}|a_p|^2) - \frac{1}{\tau_m} \right] a_m - i\omega_m\beta_m a_0^2 a_p^* + \sqrt{\frac{2}{\tau_{s,m}}} s_{m,+} \quad (2)$$

$$\frac{da_p}{dt} = \left[i\omega_p(1 - \alpha_{p0}|a_0|^2 - \alpha_{pm}|a_m|^2 - \alpha_{pp}|a_p|^2) - \frac{1}{\tau_p} \right] a_p - i\omega_p\beta_p a_0^2 a_m^* \quad (3)$$

$$s_{k,-} = \sqrt{\frac{2}{\tau_{s,k}}} a_k - s_{k,+}. \quad (4)$$

As explained in Ref. 2, the nonlinear coefficients α_{ij} and β_k depend on the specific geometry and materials, and express the strength of the nonlinear interactions. The

α_{jk} terms describe self- and cross-phase modulation effects which act to shift the cavity frequencies, while the β_k terms characterize the energy transfer (frequency conversion) between the modes. As noted in Ref. 2, these terms are constrained by energy conservation, which amounts to setting $\frac{d}{dt}(|a_0|^2 + |a_m|^2 + |a_p|^2) = 0$ (in the absence of external losses), yielding the following relation:

$$\omega_0\beta_0^* = \omega_m\beta_m + \omega_p\beta_p. \quad (5)$$

In the following sections, for simplicity, we neglect losses such as linear absorption or radiation, i.e. we assume $\tau_{s,k} = \tau_k$, and neglect nonlinear two-photon absorption,

i.e. we assume α_{ij} are strictly real (two-photon absorption effects can be minimized by selecting materials less susceptible to such processes). As noted below, these considerations do not qualitatively change our results, but merely act to slightly decrease the overall conversion efficiency once losses are included [1, 2].

The dependence of the coupling coefficients α_{ij} and β_k on the geometry of the system can be obtained via a simple perturbative calculation involving the linear eigenmodes of the cavity, as described in Ref. 2. Carrying out this procedure to first order in $\chi^{(3)}$ yields the following coupling coefficients:

$$\beta_0 = \frac{1}{8} \frac{\int d^3\mathbf{x} \epsilon_0 \chi^{(3)} [(\mathbf{E}_0^* \cdot \mathbf{E}_0^*)(\mathbf{E}_m \cdot \mathbf{E}_p) + 2(\mathbf{E}_0^* \cdot \mathbf{E}_m)(\mathbf{E}_0^* \cdot \mathbf{E}_p)]}{\left[\int d^3\mathbf{x} \epsilon |\mathbf{E}_0|^2 \right] \left[\int d^3\mathbf{x} \epsilon |\mathbf{E}_m|^2 \right]^{1/2} \left[\int d^3\mathbf{x} \epsilon |\mathbf{E}_p|^2 \right]^{1/2}} \quad (6)$$

$$\beta_m = \beta_p = \frac{1}{2} \beta_0^* \quad (7)$$

$$\alpha_{jj} = \frac{1}{8} \frac{\int d^3\mathbf{x} \epsilon_0 \chi^{(3)} [|\mathbf{E}_j \cdot \mathbf{E}_j^*|^2 + |\mathbf{E}_j \cdot \mathbf{E}_j|^2]}{\left[\int d^3\mathbf{x} \epsilon |\mathbf{E}_j|^2 \right]^2} \quad (8)$$

$$\alpha_{jk} = \frac{1}{8} \frac{\int d^3\mathbf{x} \epsilon_0 \chi^{(3)} [|\mathbf{E}_j \cdot \mathbf{E}_k|^2 + |\mathbf{E}_j \cdot \mathbf{E}_k^*|^2 + |\mathbf{E}_j|^2 |\mathbf{E}_k|^2]}{\left[\int d^3\mathbf{x} \epsilon |\mathbf{E}_j|^2 \right] \left[\int d^3\mathbf{x} \epsilon |\mathbf{E}_k|^2 \right]} \quad (9)$$

$$\alpha_{kj} = \alpha_{jk}, \quad (10)$$

where \mathbf{E}_k is the electric field in the k th mode and the denominators arise from the normalization of $|a_k|^2$. As expected, Eqs. (6–7) satisfy Eq. (5), where Eq. (5) was obtained by imposing energy conservation on the TCMT equations without reference to the specific case of Maxwell's equations.

There are six different α_{jk} parameters [three SPM (α_{jj}) and three XPM (α_{jk}) coefficients], and in general they will all differ. However, from Eqs. (8–9) we see that they are all determined by similar modal integrals, lead to frequency shifting of the cavity frequencies, and all scale as $1/V$, where V denotes a modal volume of the fields [41]. Therefore, in the following sections, we begin by neglecting the frequency-shifting terms as in Ref. 1, and then in Sec. IV C we study the essential effects of frequency shifting in the simplified case where all the coefficients are equal ($\alpha_{jk} = \alpha$). Of course, for a specific geometry one would calculate all coefficients Eqs. (6–10), but in this paper, we focus on the fundamental physics and phenomena rather than the precise behavior of a

specific geometry.

III. QUANTUM-LIMITED VS. COMPLETE CONVERSION

As described below, the DFWM process we consider here exhibits drastically different behavior depending on the ratio of $\Delta\omega$ to ω_0 . In particular, there exist at least two distinct regimes of operation, corresponding to quantum-limited ($|\Delta\omega| < \omega_0$) and complete ($\Delta\omega \geq \omega_0$) conversion. It turns out that, although our coupled-mode formalism is entirely classical, the *same* behaviors can be more easily understood by considering photon interactions in a quantum picture. Although this system is, of course, described by the general Manley-Rowe relations, which can be derived from both classical [44, 45, 48] and quantum [42, 43] arguments similar to those here, it is useful to review a basic picture of such limits and their physical consequences for the specific case of intra-cavity

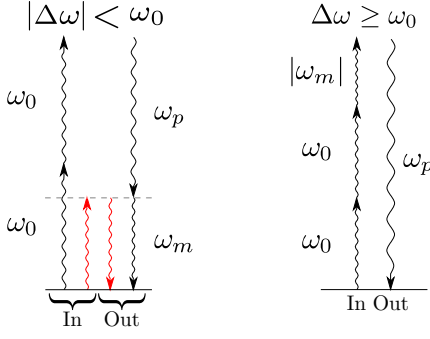


FIG. 2: (Color online) Diagram of nonlinear up-conversion process involving input light at ω_0 and ω_m and output light at ω_p and ω_m . The conversion efficiency of DFWM is determined by $\Delta\omega$, and photon energy conservation consideration (see text), leading to at least two different regimes of operation: (Left:) for $|\Delta\omega| < \omega_0$, two ω_0 pump photons and an signal ω_m photon are converted into two ω_m signal photons and an ω_p photon. The input ω_m photon is only necessary to initiate the conversion process and emerges unchanged after the interaction (indicted by red). (Right:) for $\Delta\omega \geq \omega_0$, two incoming ω_0 and a single ω_m photon are combined to produce an ω_p photon. In contrast to the previous regime, the ω_m photon is energetically needed to produce the ω_p photon.

DFWM.

Our focus in this manuscript is the up-conversion process (or interaction) corresponding to taking input light at frequencies ω_0 and ω_m and generating output light at frequency ω_p . Therefore, an appropriate figure of merit is the ratio of the output power in the ω_p mode to the total input power, which we define as the absolute efficiency $\eta = |s_{p,-}|^2 / (|s_{0,+}|^2 + |s_{m,+}|^2)$.

As described in the previous section, the coupled-mode equations [Eqs. (1–4)] follow from very general and purely classical considerations. The same considerations yield relationships between the frequencies and coupling coefficients of the problem, such as frequency conservation ($\omega_m + \omega_p = 2\omega_0$) and energy conservation ($\omega_m\beta_m + \omega_p\beta_p = \omega_0\beta_0^*$). Additional conservation rules that are perhaps best understood from quantum arguments, such as photon energy ($\hbar|\omega|$) conservation and standard $\chi^{(3)}$ selection rules [48], also play a substantial role in the physics of nonlinear frequency conversion. In the case of the DFWM up-conversion process considered here, $\chi^{(3)}$ selection rules imply that nonlinear interactions can only be initiated if there exist at least three input photons: $2\omega_0$ photons and one ω_m photon.

In the $|\Delta\omega| < \omega_0$ regime, there are at least two important features that can be understood from the above relations: First, depletion of the signal input power ($s_{m,+}$) is impossible, leading to a conversion efficiency $\eta < 1$. Second, in order to maximize the total conversion efficiency, one desires $s_{m,+}$ to be as small as possible. These features can be understood by considering a simple picture of the nonlinear photon-photon interaction, as follows. From the DFWM $\chi^{(3)}$ selection rule [48], it follows that the creation of an ω_p photon is accompanied by the destruc-

tion of two ω_0 photons and one ω_m photon. The latter, along with photon energy conservation, leads to the process considered in Fig. 2 (left), in which two ω_0 photons and an ω_m photon interact to yield two ω_m photons and an ω_p photon. From the figure, and since $2\omega_0 > \omega_p$, one can see that the incident ω_m photon (depicted in red) is merely required by the $\chi^{(3)}$ selection rule to initiate the interaction, and emerges unmodified, accompanied by an ω_p photon and an additional ω_m photon. Thus, it is clear that the input ω_m photon does not actively participate in the energy transfer and therefore merely reduces the maximum possible conversion efficiency. This implies that one desires a minimal input signal power to initiate the up-conversion. Effectively, the incident ω_m photons are amplified by the conversion process (a similar amplification effect is a crucial component in other nonlinear interactions, such as OPAs in $\chi^{(2)}$ media [48, 104, 105]). In addition, it is clear that complete depletion of the signal photons, i.e. $s_{m,-} = 0$, is not possible for non-zero $s_{m,+}$, and therefore the conversion efficiency must be less than 100% (since the total input power is conserved). No such restriction is placed on $s_{0,-}$, and therefore we expect that maximal efficiency will be obtained for arbitrarily low signal power and complete depletion of the pump power, i.e. $s_{0,-} = 0$.

Based on these arguments, we can predict the maximal efficiency of the conversion process by considering the ratio of the energy of the output ω_p photon ($\hbar\omega_p$) to the energy of the three input photons [$\hbar(2\omega_0 + \omega_m)$]. Since the ω_m photons can be provided with arbitrarily low amplitude, we therefore expect maximal efficiency to be achieved upon neglecting their contribution, i.e. we predict a maximal efficiency of:

$$\eta_{\max}(|\Delta\omega| < \omega_0) = \frac{\hbar\omega_p}{2\hbar\omega_0} = \frac{\omega_p}{2\omega_0}. \quad (11)$$

Note that this efficiency depends only on the ratio of $\Delta\omega$ to ω_0 and \hbar cancels, so it should appear in the classical limit as well. As we shall see in Sec. IV A, this prediction is verified analytically by examining the steady-state solution of our coupled-mode equations.

In the $\Delta\omega \geq \omega_0$ regime, the conversion process is fundamentally different and, in particular, complete depletion of the ω_m and ω_0 photons is possible, leading to 100% conversion efficiency. Basically, because $\omega_p > 2\omega_0$ in this case, no additional photons are required to satisfy photon energy conservation, yielding the nonlinear interaction process depicted in Fig. 2 (right), where two input ω_0 photons and an ω_m photon combine to produce an ω_p photon. Note that now the input ω_m photon actively participates in the energy transfer, in contrast to the $|\Delta\omega| < \omega_0$ regime, leading to a maximal conversion efficiency occurring when $s_{0,+}$ and $s_{m,+}$ are both non-zero. Furthermore, since ω_p is now the only product of the interaction, we expect that complete depletion of both the pump and signal powers, $s_{0,-} = s_{m,-} = 0$, should be possible, leading to 100% conversion efficiency.

As before, this can also be quantified by comparing the ratio of the output energy ($\hbar\omega_p$) to the input energy [$\hbar(2\omega_0 + |\omega_m|)$] (note that now the energy of ω_m photon is $\hbar|\omega_m|$), and the result follows from the fact that $2\omega_0 + |\omega_m| = \omega_p$. Again, we shall see in Sec. IV B, this prediction is validated analytically and directly from the coupled-mode equations, yielding also the critical input powers at which 100% conversion is achieved.

In this section, we made a number of predictions based on very general arguments relying on a quantum interpretation of the nonlinear interactions, allowing us to obtain predictions of maximal conversion efficiency. Our final results, of course, contained no factors of \hbar and it is therefore not surprising that we recover the same results (albeit with more detail, e.g. predictions of the values of critical powers) in the ensuing analysis of the purely-classical coupled-mode equations. Nevertheless, the heuristic quantum picture of Fig. 2 has the virtue of being simple and revealing, while the classical derivation is more complicated (although more quantitative). Similar quantum arguments have also proven useful in other contexts, such as in many problems involving classical radiation [106], or the recently-studied problem of optical bonding/anti-bonding in waveguide structures [107].

IV. COUPLED-MODE ANALYSIS

In order to gain a simple understanding of the system, we shall first consider frequency conversion in the absence of self- and cross-phase modulation, i.e. $\alpha_{jk} = 0$. The nonzero- α case will be considered in Sec. IV C. Section IV A focuses on the $|\Delta\omega| < \omega_0$ regime, whereas Sec. IV B focuses on the $\Delta\omega \geq \omega_0$ regime. In both cases, we describe the solutions to the coupled-mode equations [Eqs. (1–3)] in the steady state, including the stability of these solutions and their dependence on the cavity parameters.

A. $|\Delta\omega| < \omega_0$ regime: Limited conversion

Although the analysis in this section is general, for the purposes of plotting results we choose the specific parameters: $\alpha_{jk} = 0$, $\tau_0 = \tau_m = \tau_p = 100/\omega_0$, $\beta = 10^{-4}$, and $\Delta\omega = 0.05\omega_0$. The qualitative results remain unchanged as these parameters are varied, provided that the Q are large enough such that mode overlap is minimal as required by CMT. The influence of varying these parameters is discussed further at the end of the section.

To understand the stability and dynamics of the nonlinear coupled-mode equations in the quantum-limited regime, we apply the standard technique of identifying the fixed points of Eqs. (1–3) and analyzing the stability of the linearized equations around each fixed point [108]. A fixed point is given by a steady-state solution where the mode amplitudes vary as $a_k(t) = A_k e^{i\omega_k t}$, with the A_k being unknown constants. Plugging this steady-state

ansatz into Eqs. (1–3), we obtain three coupled polynomial equations in the parameters $A_0, A_m, A_p, s_{0,+}$, and $s_{m,+}$. These polynomials were solved using Mathematica to obtain the mode energies $|A_k|^2$, which are then used to calculate the efficiency $\eta = |s_{p,-}|^2 / (|s_{0,+}|^2 + |s_{m,+}|^2)$. The phases of the A_k can be easily determined from the steady-state equations of motion; A_0 and A_m acquire the phases of $s_{0,+}$ and $s_{m,+}$ respectively, while the phase of A_p is that of $\beta_p A_0^2 A_m^*$ rotated by $\pi/2$. Without loss of generality, $s_{0,+}$ and $s_{m,+}$ can be chosen to be real.

In general, this system has either one or three solutions, only one of which is ever stable. The stability and efficiency of this solution are shown in Fig. 3 for the specific parameters mentioned above. We observe that maximal conversion efficiency is obtained in the limit as input signal power $s_{m,+}$ is reduced to zero, consistent with the discussion in the previous section. To obtain the maximum efficiency and the corresponding critical input powers, complete depletion of the pump (ω_0) photon is required, i.e. $s_{0,-} = 0$ (note that one cannot require depletion of the signal photon, for the reasons discussed in the previous section). We find that the maximum efficiency η_{\max} is obtained at $|s_{0,+}^{\text{crit}}|^2 = P_0$ as $|s_{m,+}|^2 \rightarrow 0$, where:

$$P_0 = \frac{4}{\tau_0 |\beta_0| \sqrt{\tau_m \tau_p |\omega_m \omega_p|}} \quad (12)$$

$$\eta_{\max} = \frac{\omega_p}{2\omega_0} = \frac{1}{2} \left(1 + \frac{\Delta\omega}{\omega_0} \right), \quad (13)$$

Note that Eq. (13) is identical to the value predicted in the previous section. In the important case of narrow-band conversion, $|\Delta\omega| \ll \omega_0$, the maximum efficiency is approximately 50%. (however, this is relative to the pump power— compared to the input signal alone, the output signal is amplified to an arbitrary degree). If $Q_0 \sim Q_m \sim Q_p$, then, as in THG [1], the critical power scales as V/Q^2 , where V is the modal volume (recall that $\beta \sim 1/V$).

As $\Delta\omega \rightarrow \omega_0$, the maximum efficiency approaches unity, i.e. 100% conversion can be achieved in the limit. This limit is reminiscent of second-harmonic generation, since $\omega_p = 2\omega_0$. However, the interaction process is fundamentally different from the standard ($\chi^{(2)}$) SHG in a number of ways. First, one is converting DC ($\omega_m \approx 0$) light and ω_0 pump light into $2\omega_0$. Second, the stability of this solution (described below) is quite different from that of SHG [46, 47, 82]. Finally, the critical power in this case, P_0 , diverges as $1/\sqrt{1 - (\Delta\omega/\omega_0)^2}$ for $\Delta\omega$ near ω_0 . However, $\Delta\omega$ close but not equal to ω_0 yields a reasonable P_0 : for example, $\Delta\omega = 0.95\omega_0$ yields efficiency $\eta = 0.975$ with a critical power roughly three times the critical power for $\Delta\omega$ near zero. Because this near-“SHG” situation involves coupling resonances at very different frequency scales, it is reminiscent of using $\chi^{(2)}$ DFG to produce THz from infrared [60].

Eqs. (12–13) are only valid in the limit $|s_{m,+}|^2 \rightarrow 0$, which is ideal from an efficiency perspective. How-

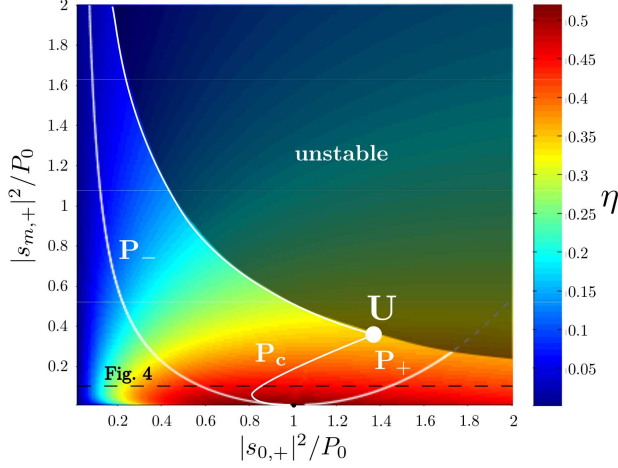


FIG. 3: (Color online) Color plot of the steady-state conversion efficiency $\eta = |s_{p,-}|^2 / (|s_{0,+}|^2 + |s_{m,+}|^2)$ as a function of input power $|s_{0,+}|^2$ and $|s_{m,+}|^2$, for a system consisting of $\Delta\omega = 0.05\omega_0$, $\beta = 10^{-4}$, and $\tau_0 = \tau_p = 100$. Both powers are normalized by the critical power $P_c(|s_{m,+}|^2 \rightarrow 0) = P_0 = 2/\tau_0|\beta|\sqrt{\tau_m\tau_p|\omega_m\omega_p|}$ (black dot). The shaded region indicates that the solution is unstable. The curves P_{\pm} indicate the powers at which depletion of the ω_0 input light is achieved, i.e. $s_{0,-} = 0$; the critical power $P_c(|s_{m,+}|^2)$ is defined as the total input power that yields the highest *stable* efficiency for any given $|s_{m,+}|^2$. The dash line is the cross-section shown in Fig. 4.

ever, it is interesting to consider the system for non-infinitesimal $s_{m,+}$, in which case we solve for the input power that yields a stable solution with maximal efficiency for a given $s_{m,+}$. We denote this input power by $P_c(|s_{m,+}|^2) = |s_{0,+}^{\text{crit}}|^2 + |s_{m,+}|^2$, where $|s_{0,+}^{\text{crit}}|^2$ (a function of $|s_{m,+}|^2$) is defined to be the pump power required to achieve maximum, stable conversion efficiency for a given signal power $|s_{m,+}|^2$. As seen in Fig. 3, this efficiency is always $\leq \eta_{\text{max}}$, and $P_c \rightarrow P_0$ as $s_{m,+} \rightarrow 0$. In the non-zero $|s_{m,+}|^2$ regime, P_c does not correspond to complete depletion of the pump. Requiring pump depletion ($s_{0,-} = 0$) for a given signal power $|s_{m,+}|^2$ yields two pump powers, which we label $P_{\pm}(|s_{m,+}|^2)$. $P_+(|s_{m,+}|^2)$ does indeed provide a solution with maximal efficiency, however this solution is always unstable. As seen from Fig. 3, only for small signal power $s_{m,+}$ does depletion of the pump lead to maximal efficiency.

In general, to obtain the largest efficiency while retaining stability, one would aim to operate with low signal power $|s_{m,+}|^2$ and use a pump power near the critical power P_0 given in Eq. (12). However, it is interesting to consider the unstable solutions, because they turn out to be related to limit cycles. As mentioned above, the system contains either one or three steady-state solutions for given input powers. Fig. 4 plots these stable and unstable solutions as a function of pump power $|s_{0,+}|^2$ at fixed signal power $|s_{m,+}|^2 = 0.1P_0$, corresponding to the horizontal dashed line in Fig. 3. For low input pump

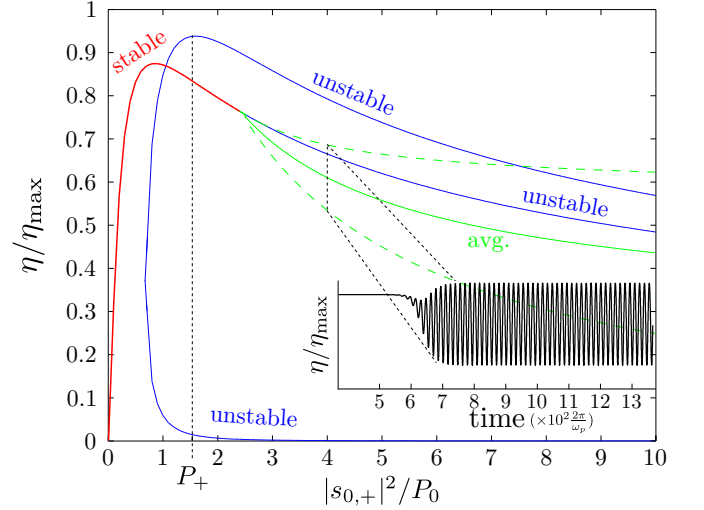


FIG. 4: (Color online) Bifurcation diagram of the steady-state efficiency η , normalized by the quantum-limited maximum efficiency $\eta_{\text{max}} = \frac{1}{2}\omega_p/\omega_0$, as a function of $|s_{0,+}|^2$, normalized by P_0 , for signal power $|s_{m,+}|^2 = 0.1P_0$ (indicated by the black dashed line of Fig. 3). Red/blue correspond to a stable/unstable solution (note that the two bifurcating solutions are always unstable). The green dashed line illustrates the bounds of the limit cycles obtained from time domain simulations, where the solid green line yields the average over the cycle. (Inset:) Efficiency as a function of time in units of the period $T_p = 2\pi/\omega_p$ in a regime where there exists a limit cycle.

power $|s_{0,+}|^2$, the system has a single steady-state solution; as the pump power is increased, the system experiences a bifurcation yielding two unstable solutions. As mentioned above, the higher efficiency solution emerging from the bifurcation achieves a maximum corresponding at $|s_{0,+}|^2 = P_+$, coinciding with complete depletion of the pump ($s_{0,-} = 0$), but this maximal efficiency solution is always unstable; note that there may be a stable solution at $|s_{0,+}|^2 = P_+$, but the stable solution will have a lower efficiency than the maximal, unstable solution, as shown in Fig. 4. Furthermore, the original stable solution eventually becomes unstable as the pump power is increased (this can occur before or after the bifurcation, depending on the system parameters); this onset of instability coincides with the onset of limit cycles, stable oscillating-efficiency solutions. An example of these limit cycles are shown in Fig. 4, where the green dashed lines indicate the bounds of the oscillations and the solid green line gives the average. The limit cycles are plotted as a function of time in the inset of Fig. 4. The limit cycles shown here were obtained by numerically time-evolving the coupled-mode equations. In general, we find that these limit cycles oscillate with a period proportional to τ_p .

Figures 3–4 describe a system corresponding to a particular set of values for the parameters $\Delta\omega$ and τ_k . Qualitatively, the most important features of the figures remain largely unchanged as these parameters are var-

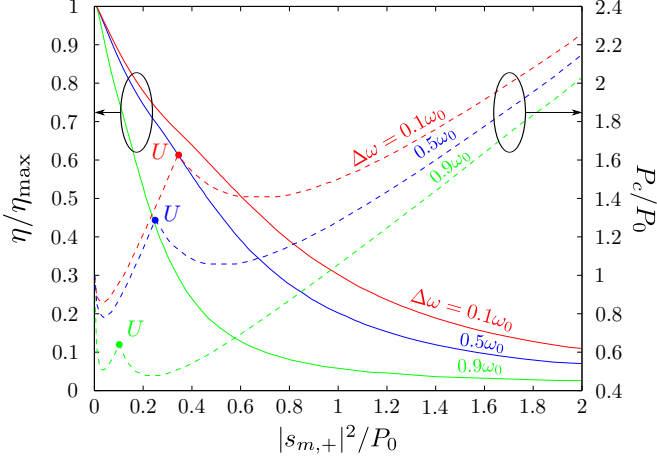


FIG. 5: (Color online) Plot of the steady-state efficiency η (solid lines) along the critical solution [total input power $P_c(|s_{m,+}|^2) = |s_{m,+}|^2 + |s_{0,+}^c|^2$ that yields the maximum efficiency for a given $|s_{m,+}|^2$ (solid white curve of Fig. 3)] and the value of P_c (dashed lines) as a function of $|s_{m,+}|^2$, normalized by P_0 , for three different values of $\Delta\omega$: $0.1\omega_0$ (red), $0.5\omega_0$ (blue), and $0.9\omega_0$ (green). The kinks in the P_c curves correspond to the point U where P_c reaches the region of instability (see Fig. 3). The coupling lifetimes τ and coefficient β of the system are equivalent to those of Fig. 3.

ied. Basically, there exist at most three solutions to the coupled-mode equations, one of which has a finite region of stability as a function of $s_{0,+}$ and $s_{m,+}$, with the general shape that is shown in Fig. 3, and two others that are always unstable and bifurcate at a finite $s_{0,+}$. There are however, some differences to note: First, as $\Delta\omega$ increases from 0, the maximum steady-state efficiency also increases, asymptoting to $\eta = 1$ as $\Delta\omega \rightarrow \omega_0$. This was obtained analytically and is quantified in Eq. (13). Unfortunately, we find that as $\Delta\omega$ increases, the region of instability in Fig. 3 also increases, and furthermore, the conversion efficiency at finite $s_{m,+}$ also drops off more rapidly. (In particular, we observe in the “SHG” limit of $\Delta\omega \rightarrow \omega_0$, the system becomes largely unstable except for very low signal powers.) These tendencies are depicted in Fig. 5, which plots $P_c(|s_{m,+}|^2)$ and the corresponding conversion efficiency for different values of $\Delta\omega$. The kinks observed in the plots of P_c are due to the discontinuity in the slope of the P_c curve as it reaches the region of instability, corresponding to the point U in Fig. 3.

Varying τ_k does not affect the maximum possible efficiency and also leaves Fig. 3 qualitatively unchanged, changing only the scale of the critical input power P_0 . The stability of the system however, does depend on the relative lifetimes of the cavity modes. In particular, the stability depends largely on the ratio τ_0/τ_p , and decreases weakly as τ_m increases with respect to either τ_0 or τ_p . This makes sense since, as argued in Sec. III, the ω_m photons do not actively participate in the energy transfer. (A similar dependence on the ratio of the lifetimes

was also observed in the case of THG [1].) More quantitatively, we follow the position of the point U (the point where P_c reaches the region of instability) as the τ_k are varied. Assuming equal modal lifetimes ($\tau_0 = \tau_m = \tau_p$ as in Fig. 3), we find that U lies at critical input powers $|s_{0,+}|^2 \approx 1.28P_0$ and $|s_{m,+}|^2 \approx 0.35P_0$. Increasing τ_0/τ_p , from 1 to 10, we find that U moves to $|s_{0,+}|^2 \approx 10P_0$ and $|s_{m,+}|^2 \approx 4.75P_0$. However, if we instead keep $\tau_0 = \tau_p$ and increase τ_m such that $\tau_m/\tau_0 = \tau_m/\tau_p = 10$, U moves only to $|s_{0,+}|^2 \approx 1.05P_0$ and $|s_{m,+}|^2 \approx 0.27P_0$. Note that, as mentioned previously, maximal stable conversion efficiency is obtained for low signal power $|s_{m,+}|^2$ and input power $|s_{0,+}|^2$ near the critical power P_0 , regardless of τ_k . We note that rescaling β simply scales the input power and therefore changing β does not affect the dynamics.

Thus far, we have focused on the up-conversion process: taking input light at frequencies ω_0 and ω_m and generating output light at frequency $\omega_p > \omega_0$. However, it suffices to consider the above system when $\Delta\omega < 0$ to understand the physics of the alternative, down-conversion process: taking input light at frequencies ω_0 and ω_p and generating output light at frequency ω_m . For $\Delta\omega < 0$, we effectively have $\omega_m \leftrightarrow \omega_p$. In this regime, all of the above analysis holds, and in particular, the maximal efficiency, given by Eq. (13), is obtained as $|s_{m,+}|^2 \rightarrow 0$ with $|s_{0,+}|^2 = P_0$. Similarly, the stability of the solutions follow similar trends to those outlined above.

B. $\Delta\omega \geq \omega_0$ regime: Complete conversion

When $\Delta\omega$ is larger than ω_0 , we argued in Sec. III that the system is capable of complete conversion, i.e. $\eta = 1$. In this section, we demonstrate the existence of a critical steady-state solution to the classical coupled mode equations with complete conversion and analyze the stability of this critical solution, as well as relate DFWM to our previous work on THG [1, 2].

As in the previous section, we consider the equations of motion Eqs. (1–3) in the steady state. To obtain the critical solution, we again require depletion of the pump power, i.e. $s_{0,-} = 0$. However, as argued in Sec. III, complete depletion of the signal, $s_{m,-} = 0$ must also occur. Recall from Sec. III that complete ω_m depletion is possible in the $\Delta\omega \geq \omega_0$ regime since the up-conversion process does not produce ω_m photons (see Fig. 2). Imposing the depletion constraints on the steady-state equations of motion yields the following critical cavity energies $|a_k^{\text{crit}}|^2$:

$$|a_0^{\text{crit}}|^2 = \frac{1}{|\beta_m| \sqrt{\tau_m \tau_p} |\omega_m \omega_p|}, \quad (14)$$

$$|a_m^{\text{crit}}|^2 = \frac{\tau_m |\omega_m|}{2\tau_0 \omega_0} |a_0^{\text{crit}}|^2, \quad (15)$$

$$|a_p^{\text{crit}}|^2 = \frac{\tau_p \omega_p}{2\tau_0 \omega_0} |a_0^{\text{crit}}|^2, \quad (16)$$

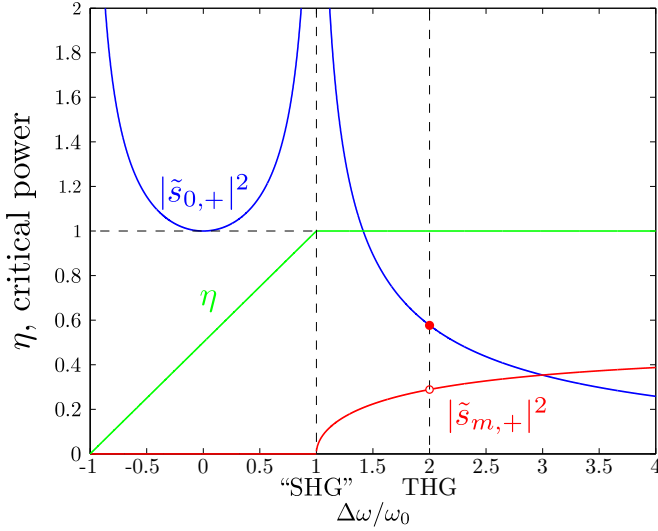


FIG. 6: (Color online) Plot of the critical powers $|\tilde{s}_{0,+}|^2$ (blue), $|\tilde{s}_{m,+}|^2$ (red), and maximum steady-state efficiency η (green) as a function of $\Delta\omega/\omega_0$ (the tilde over the critical powers indicates that the values have been rescaled by the factor $4/\tau_0|\beta_0|\sqrt{\tau_m\tau_p\omega_0^2}$). The vertical dashed lines at $\Delta\omega = \omega_0$ and $\Delta\omega = 2\omega_0$ indicate special degenerate regimes, corresponding to “second harmonic generation” (SHG) and third harmonic generation (THG). (Note the discontinuity in $|\tilde{s}_{m,+}|^2$ located at $\Delta\omega = 2\omega_0$, explained in the text).

which lead to the following critical powers:

$$|s_{0,+}^{\text{crit}}|^2 = P_0 \quad (17)$$

$$|s_{m,+}^{\text{crit}}|^2 = \frac{|\omega_m|}{2\omega_0} P_0, \quad (18)$$

where P_0 is given by Eq. (12). Solving for the corresponding output signal $|s_{p,-}|^2$, the output power is indeed 100% of the input power, as required by energy conservation. (In contrast, the assumption that $s_{0,-} = s_{m,-} = 0$ in the $|\Delta\omega| < \omega_0$ case yields no solution). Note that the critical signal power $|s_{m,+}^{\text{crit}}|^2$ is now non-zero, due to the fact that the energy from the signal ω_m photons is necessary to produce the output ω_p photons. This is in contrast with the $|\Delta\omega| < \omega_0$ regime where maximal conversion efficiency was only achieved in the limit as input signal power $|s_{m,+}|^2$ decreased to zero. The critical pump and signal powers, with the corresponding maximum efficiency η , are plotted versus $\Delta\omega$ in Fig. 6 for both $\Delta\omega$ regimes.

As may be noted from Fig. 6, there are two particular values of $\Delta\omega$ that warrant special attention when $\Delta\omega \geq \omega_0$. The first case, when $\Delta\omega = \omega_0$, the “SHG” case, was discussed in the previous section. The second case is when $\Delta\omega = 2\omega_0$. In this case, $\omega_m = -\omega_0$ and $\omega_p = 3\omega_0$, reminiscent of third-harmonic generation (THG). In fact, this case of DFWM corresponds exactly to $\chi^{(3)}$ THG, and thus $\Delta\omega > \omega_0$ strictly generalizes our previous THG analysis [1]. To see this, some care must be taken to adjust the coupling coefficients β_k given in

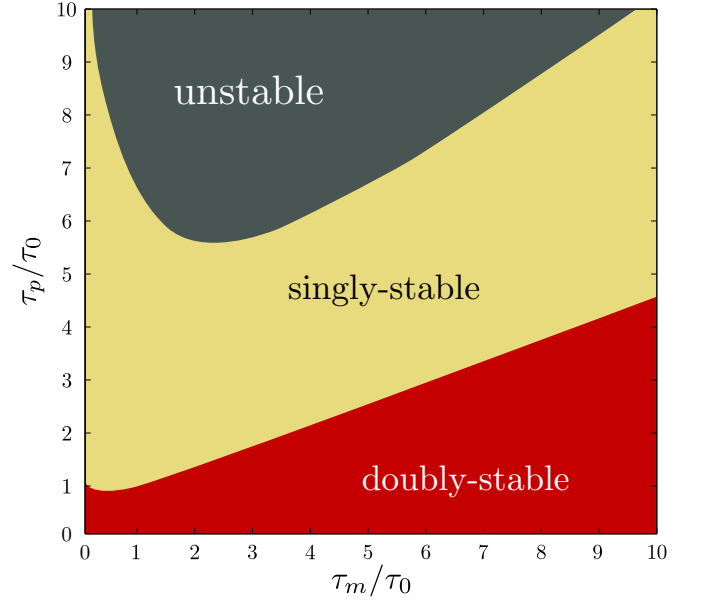


FIG. 7: (Color online) Stability contours (number of stable solutions) as a function of modal lifetimes τ_m and τ_p , normalized by τ_0 , pumping at the critical input powers $|s_{0,+}^{\text{crit}}|^2$ and $|s_{m,+}^{\text{crit}}|^2$. The stability in the $\Delta\omega \geq \omega_0$ regime is independent of the value of $\Delta\omega$.

Eqs. (6–7) to properly implement the rotating wave approximation; since $\omega_m = -\omega_0$, we have that $a_m = a_0^*$, and thus $\beta_0 \rightarrow \beta_0 + \beta_m^*$ and $\beta_m \rightarrow \beta_m + \beta_0^*$. This results in $\beta_0 = \beta_m^* = 3\beta_p^*$, exactly as shown in [1]. Furthermore, we have $|s_{0,+}^{\text{crit}}|^2 = |s_{m,+}^{\text{crit}}|^2 = P_0$ (note that this differs by a factor of two from Eq. (18), due to the adjusted β_k values); upon requiring that $\tau_0 = \tau_m$, this recovers the critical power previously obtained for THG [1]. Note that the correspondence between $\Delta\omega = 2\omega_0$ and $\chi^{(3)}$ THG is exact, whereas the $\Delta\omega = \omega_0$ limit has little in common with $\chi^{(2)}$ SHG as discussed above.

The existence of an $s_{0,-} = s_{m,-} = 0$ solution having demonstrated the existence of critical powers where 100% conversion can be achieved, we are now interested in characterizing the system at this critical power by studying all of the fixed points. These fixed points were obtained using Mathematica as in the previous section, and their stability was determined via linear stability analysis as before. For the critical input power, the steady-state equations of motion yield three solutions; however, in contrast to the $|\Delta\omega| < \omega_0$ regime, there exists multistability when $\Delta\omega \geq \omega_0$. Similar to the case of THG ($\Delta\omega = \omega_0$), the system is either singly stable, doubly stable, or unstable, depending on the values of the mode lifetimes τ_k (see Fig. 7). In this $\Delta\omega > \omega_0$ regime, the stability of the solutions does not depend on $\Delta\omega$, again in contrast with the quantum-limited regime. Unlike the $|\Delta\omega| < \omega_0$ regime, the value of τ_m now plays a significant role in the stability of the solutions.

C. Self- and Cross-Phase Modulation ($\alpha \neq 0$)

Finally, we briefly consider the effects of SPM and XPM. This corresponds to taking the coefficients α_{jk} to be non-zero; as mentioned above, for simplicity, we take all the coefficients to be equal, i.e. $\alpha_{jk} = \alpha$ for all j, k . The main effect of SPM and XPM in Eqs. (1–2) is to shift the resonant frequencies of the cavity in proportion to the energy of the modes in the cavity. Generally, this drives the frequency input light off resonance and therefore degrades the overall conversion efficiency obtained in Secs. IV A and IV B, as shown in Ref. 1. However, in Ref. 1, we showed that one simple way to overcome this difficulty is to pre-shift the cavity resonant frequencies so as to compensate for the SPM/XPM effects when operating near the critical input power. Unfortunately, this will inevitably affect the stability analysis obtained in the $\alpha = 0$ case, and therefore a new analysis that includes SPM/XPM effects must be performed. In this remainder of this section, we only analyze the stability of the maximal-efficiency solutions obtained in Secs. IV A and IV B, and in particular, we find that 100% photon-conversion efficiency can be obtained in this case as well.

The change in cavity frequency due to SPM/XPM can be accounted for by a pre-shifting technique described in Ref. 1. In particular, the α terms in Eqs. (1–3) act to shift the cavity resonant frequencies from $\omega_k^{\text{cav}} \rightarrow \omega_k^{\text{NL}}$, spoiling the frequency-conservation relations necessary for efficient nonlinear frequency conversion as well as detuning the resonances from the input light. However, one can simply design the cavity frequencies to be resonant at the shifted frequencies, i.e. $\omega_k^{\text{cav}} = \omega_k^{\text{NL}}$, for a given steady-state solution. For the critical solutions corresponding to 100% photon-conversion efficiency, this implies that the new cavity frequencies will be given by [1]:

$$\omega_0^{\text{cav}} = \frac{\omega_0}{1 - \alpha(|a_0^{\text{crit}}|^2 + |a_m^{\text{crit}}|^2 + |a_p^{\text{crit}}|^2)} \quad (19)$$

$$\omega_m^{\text{cav}} = \frac{\omega_m}{1 - \alpha(|a_0^{\text{crit}}|^2 + |a_m^{\text{crit}}|^2 + |a_p^{\text{crit}}|^2)} \quad (20)$$

$$\omega_p^{\text{cav}} = \frac{\omega_p}{1 - \alpha(|a_0^{\text{crit}}|^2 + |a_m^{\text{crit}}|^2 + |a_p^{\text{crit}}|^2)}, \quad (21)$$

where $|a_k^{\text{crit}}|^2$ are the energies of the modes at critical power. For cavities resonances ω_k^{cav} , the new equations

of motion are given by:

$$\begin{aligned} \frac{da_0}{dt} = & \left[i\omega_0^{\text{cav}}(1 - \alpha_{00}|a_0|^2 - \alpha_{0m}|a_m|^2 - \alpha_{0p}|a_p|^2) \right. \\ & \left. - \frac{1}{\tau_0} \right] a_0 - i\omega_0\beta_0 a_0^* a_m a_p + \sqrt{\frac{2}{\tau_{s,0}}} s_{0,+} \end{aligned} \quad (22)$$

$$\begin{aligned} \frac{da_m}{dt} = & \left[i\omega_m^{\text{cav}}(1 - \alpha_{m0}|a_0|^2 - \alpha_{mm}|a_m|^2 - \alpha_{mp}|a_p|^2) \right. \\ & \left. - \frac{1}{\tau_m} \right] a_m - i\omega_m\beta_m a_0^2 a_p^* + \sqrt{\frac{2}{\tau_{s,m}}} s_{m,+} \end{aligned} \quad (23)$$

$$\begin{aligned} \frac{da_p}{dt} = & \left[i\omega_p^{\text{cav}}(1 - \alpha_{p0}|a_0|^2 - \alpha_{pm}|a_m|^2 - \alpha_{pp}|a_p|^2) \right. \\ & \left. - \frac{1}{\tau_p} \right] a_p - i\omega_p\beta_p a_0^2 a_m^*, \end{aligned} \quad (24)$$

Note that the frequencies ω_k multiplying the β_k terms do not need to be shifted, since the terms introduced by such a shifting will be higher order in $\chi^{(3)}$. By inspection, we observe that the solutions obtained in Secs. IV A and IV B at critical input power a_k^{crit} are also solutions of Eqs. (22–23), but as explained above, their stability may change. Using the results from Secs. IV A and IV B, we now study the stability properties of these solutions in the two $\Delta\omega$ regimes.

We first consider the $\Delta\omega \leq \omega_0$ regime. As in Sec. IV A, we restrict our analysis to a specific parameter regime ($\tau_0 = \tau_m = \tau_p = 100/\omega_0$, $\beta = 10^{-4}$, and $\Delta\omega = 0.05\omega_0$) for simplicity, although our qualitative conclusions apply to other parameter ranges. As discussed above in Sec. IV A, the maximal efficiency is obtained for input light with $|s_{0,+}|^2 = P_0$ as $|s_{m,+}|^2 \rightarrow 0$. Since one must always pump with finite $|s_{m,+}|^2$, and there are no analytic solutions in this case, we solve for the field energies $|a_k^{\text{crit}}|^2$ numerically at a small $|s_{m,+}|^2$ and for $|s_{0,+}|^2 = P_0$ in the case of $\alpha = 0$ in order to compute the shifted frequencies Eqs. (19–21). This allows us to solve the coupled-mode equations Eqs. (22–23) and therefore obtain the steady-state field amplitudes and phases. As in Ref. 1, the inclusion of self- and cross-phase modulation introduces new steady-state solutions absent in the $\alpha = 0$ case, and the stability of the old and new solutions are then examined again via a linear stability analysis, as in Sec. IV A. In particular, we find that the inclusion of SPM/XPM does not destroy the stability of the maximal efficiency solution in the $\alpha = 0$ case studied in Sec. IV A, and in fact creates additional stable solutions, as shown in Fig. 8.

A similar analysis can be performed in the $\Delta\omega > \omega_0$ regime, where it is possible to obtain the analytic form of the maximal efficiency solutions [Eqs. (14–16) in Sec. IV B]. We find that, as in the previous regime, the presence of α introduces additional stable solutions, while retaining the original 100% efficiency $\alpha = 0$ solution, over finite regions of the parameter space.

The presence of SPM/XPM in our system provides an opportunity to observe rich and interesting dynamical

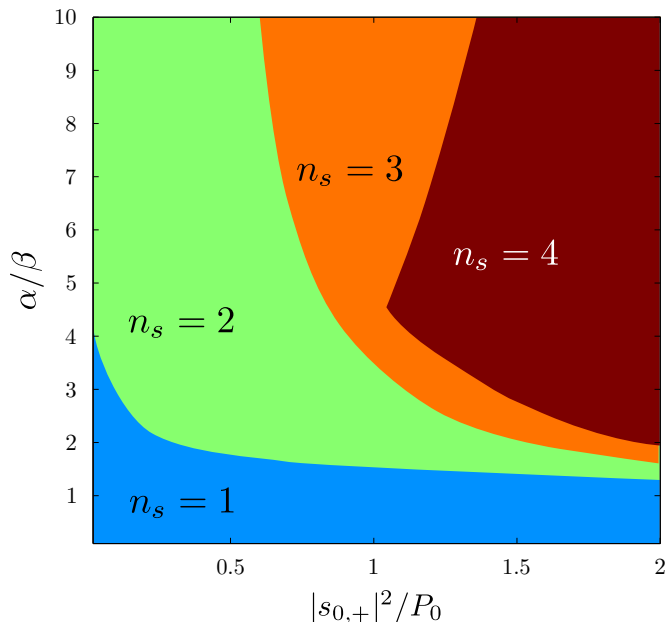


FIG. 8: (Color online) Contour plot of number of stable solutions (n_s) as a function of α/β and $|s_{0,+}|^2/P_0$, for input pump power $|s_{m,+}|^2 = 0.1P_0$, and for the system described in the text.

behaviors, including limit cycles and hysteresis effects, that we do not explore in this paper. As noted in this section, the inclusion of these effects is not prohibitive for 100% nonlinear frequency conversion although predicting which parameter regimes allow for such conversion will depend on the system under question. In the future, we plan to examine SPM/XPM effects in more detail for realistic geometries with realistic values of α_{ij} and β_i . As in Ref. 1, the presence of multiple stable solutions means that the manner in which the source is initiated will determine which solution is excited, but a simple initialization procedure similar to that in Ref. 1 should be possible to excite the maximal-efficiency solution.

V. CONCLUSION

By exploiting a simple but rigorous coupled-mode theory framework, we have demonstrated the possibility of

achieving highly-efficient (low-power) DWFm in triply-resonant cavities, similar to our previous work in SHG and THG [1, 2]. We conclude that there are two main regimes of operation, determined by the ratio of $\Delta\omega$ to ω_0 . In particular, whereas the maximal efficiency obtainable in the $\Delta\omega \leq \omega_0$ regime, corresponding to conversion between closely-spaced resonances, is bounded above by a quantum-limited process, there is no such bound when $\Delta\omega > \omega_0$. In both regimes, a suitable choice of system parameters leads to stable, maximal-efficiency nonlinear frequency conversion, even in the presence of SPM and XPM effects. We remark that all of the results obtained in this paper correspond to the idealized case of lossless interactions, since the main focus of the paper is in examining the basic considerations involved in operating with these systems rather than predicting results for specific experimentally-relevant systems. Nevertheless, based on our previous experience with SHG and THG [1, 2], we expect that linear and nonlinear losses, e.g. coming from radiation or material absorption, will only act to slightly decrease the overall conversion efficiency and will not affect the qualitative predictions here. In a future manuscript, we plan to explore DFWm in a realistic geometry such as a ring resonator coupled to an index-guided waveguide and study some of the dynamical effects arising from SPM/XPM.

Acknowledgments

This work was supported by the MRSEC Program of the NSF under Award No. DMR-0819762 and by the U.S.A.R.O. through the ISN under Contract No. W911NF-07-D-0004. We are also grateful to Jorge Bravo-Abad at U. Autnoma de Madrid for helpful discussions.

-
- [1] H. Hashemi, A. W. Rodriguez, J. D. Joannopoulos, M. Soljacic, and S. G. Johnson, *Phys. Rev. A* **79**, 013812 (2009).
 - [2] A. Rodriguez, M. Soljačić, J. D. Joannopoulos, and S. G. Johnson, *Opt. Express* **15**, 7303 (2007).
 - [3] B. E. A. Saleh and M. C. Teich, *Fundamentals of Photonics* (Wiley, 1991).
 - [4] J. U. Fürst, D. V. Strekalov, D. Elser, M. Lassen, U. L. Andersen, C. Marquardt, and G. Leuchs, *Phys. Rev. Lett.* **104**, 153901 (2010).
 - [5] M. Bieler, *IEEE J. Sel. Top. Quant. Elec.* **14**, 458 (2008).
 - [6] R. E. Hamam, M. Ibanescu, E. J. Reed, P. Bermel, S. G. Johnson, E. Ippen, J. D. Joannopoulos, and M. Soljacic, *Opt. Express* **12**, 2102 (2008).
 - [7] I. B. Burgess, Y. Zhang, M. W. McCutcheon, A. W. Rodriguez, J. Bravo-Abad, S. G. Johnson, and M. Loncar, *Opt. Express* **17**, 20099 (2009).

- [8] J. Bravo-Abad, A. W. Rodriguez, J. D. Joannopoulos, P. T. Rakich, S. G. Johnson, and M. Soljacic, *Appl. Phys. Lett.* **96**, 101110 (2010).
- [9] J. Hald, *Optics Communications* **197**, 169 (2001).
- [10] R. Lifshitz, A. Arie, and A. Bahabad, *Phys. Rev. Lett.* **95**, 133901 (2005).
- [11] B. Freedman, G. Bartal, M. Segev, R. Lifshitz, D. N. Christodoulides, and J. W. Fleischer, *Nature* **440**, 1166 (2006).
- [12] Y. A. Morozov, I. S. Nefedov, V. Y. Aleshkin, and I. V. Krasnikova, *Semiconductors* **39**, 113 (2005).
- [13] T. J. Kippenberg, S. M. Spillane, and K. J. Vahala, *Phys. Rev. Lett.* **93**, 083904 (2004).
- [14] P. Bermel, A. Rodriguez, J. D. Joannopoulos, and M. Soljacic, *Phys. Rev. Lett.* **99**, 053601 (2007).
- [15] J. Bravo-Abad, A. W. Rodriguez, P. Bermel, S. G. Johnson, J. D. Joannopoulos, and M. Soljačić, *Opt. Express* **15**, 16161 (2007).
- [16] M. M. Fejer, *Phys. Today* **47**, 25 (1994).
- [17] V. S. Ilchenko, A. A. Savchenkov, A. B. Matsko, and L. Maleki, *Phys. Rev. Lett.* **92**, 043903 (2004).
- [18] F. S. Felber and J. H. Marburger, *Appl. Phys. Lett.* **28**, 731 (1976).
- [19] A. Parini, G. Bellanca, S. Trillo, M. Conforti, A. Locatelli, and C. De Angelis, *J. Opt. Soc. Am. B* **24**, 2229 (2007).
- [20] H. M. Gibbs, *Optical Bistability: Controlling Light with Light* (Academic Press, Orlando, FL, 1985).
- [21] A. R. Cowan and J. F. Young, *Phys. Rev. E* **68**, 046606 (2003).
- [22] M. Soljacic, M. Imabenscu, S. G. Johnson, J. D. Joannopoulos, and Y. Fink, *Opt. Lett.* **28**, 516 (2003).
- [23] M. F. Yanik, S. Fan, and M. Soljacic, *Appl. Phys. Lett.* **83**, 2739 (2003).
- [24] G. S. Dutta and J. Jolly, *Pranama-journal of Physics* **50**, 239 (1988).
- [25] Q. F. Xu and M. Lipson, *Opt. Lett.* **31**, 341 (2006).
- [26] M. Soljačić, M. Ibanescu, S. G. Johnson, Y. Fink, and J. D. Joannopoulos, *Phys. Rev. E Rapid Commun.* **66**, 055601(R) (2002).
- [27] E. Centeno and D. Felbacq, *Phys. Rev. B* **62**, R7683 (2000).
- [28] T. Tanabe, M. Notomi, S. Mitsugi, A. Shinya, and E. Kuramochi, *Opt. Lett.* **30**, 2575 (2005).
- [29] M. Notomi, A. Shinya, S. Mitsugi, G. Kira, E. Kuramochi, and T. Tanabe, *Opt. Express* **13**, 2678 (2005).
- [30] A. Dorsel, J. McCullen, P. Meystre, E. Vignes, and H. Walther, *Phys. Rev. Lett.* **51**, 1550 (1983).
- [31] K. Y. Billah and M. Shinozuka, *Phys. Rev. A* **42**, 7492 (1990).
- [32] K. J. Vahala, *Nature* **424**, 839 (2003).
- [33] M. Ferrera, D. Duchesne, L. Razzari, M. Peccianti, R. Morandotti, P. Cheben, S. Janz, D. X. Xu, B. E. Little, S. Chu, et al., *OE* **17**, 14098 (2009).
- [34] M. Ferrera, L. Razzari, D. Duchesne, R. Morandotti, Z. Yang, M. Liscidini, J. E. Sipe, S. Chu, B. E. Little, and D. J. Moss, *Nature Photonics* **2**, 737 (2008).
- [35] A. C. Turner, M. A. Foster, A. L. Gaeta, and M. Lipson, *OE* **16**, 4881 (2008).
- [36] J. E. Heebner, N. N. Lepeshkin, A. Schweinsberg, G. W. Wicks, R. W. Boyd, R. Grover, and P. T. Ho, *OL* **29**, 769 (2004).
- [37] P. P. Absil, J. V. Hryniewicz, B. E. Little, P. S. Cho, R. A. Wilson, L. G. Joneckis, and P. T. Ho, *OL* **25**, 554 (2000).
- [38] I. H. Agha, Y. Okawachi, M. A. Foster, J. E. Sharping, and A. L. Gaeta, *PRA* **76**, 043837 (2007).
- [39] D. H. Broaddus, M. A. Foster, I. H. Agha, J. T. Robinson, M. Lipson, and A. L. Gaeta, *Opt. Express* **17**, 5998 (2009).
- [40] D. Duchesne, L. Razzari, M. Ferrera, R. Morandotti, S. Chu, B. Little, and D. Moss, in *Optical Fiber Communication (OFC), collocated National Fiber Optic Engineers Conference, 2010 Conference on (OFC/NFOEC)* (2010), pp. 1–3.
- [41] J. D. Joannopoulos, S. G. Johnson, J. N. Winn, and R. D. Meade, *Photonic Crystals: Molding the Flow of Light* (Princeton University Press, 2008), 2nd ed., URL <http://ab-initio.mit.edu/book>.
- [42] M. T. Weiss, *Proc. IRE* **45**, 1012 (1957).
- [43] J. Brown, *EL* **1**, 23 (1965).
- [44] H. A. Haus, *Waves and Fields in Optoelectronics* (Prentice-Hall, Englewood Cliffs, NJ, 1984).
- [45] H. A. Haus and W. Huang, *Proc. of the IEEE* **79**, 1505 (1991).
- [46] P. D. Drummond, K. J. McNeil, and D. F. Walls, *Optica Acta* **27**, 321 (1980).
- [47] K. Grygiel and P. Szlatchetka, *Opt. Comm.* **91**, 241 (1992).
- [48] R. W. Boyd, *Nonlinear Optics* (Academic Press, California, 1992).
- [49] H. M. Gibbs, G. Khitrova, and N. Peyghambarian, *Nonlinear Photonics* (Spring-Verlag, 1990).
- [50] R. G. Smith, *IEEE J. Quantum Electron.* **6**, 215 (1970).
- [51] L.-A. Wu, M. Xiao, and H. J. Kimble, *JOSA-B* **4**, 1465 (1987).
- [52] Z. Y. Ou and H. J. Kimble, *Opt. Lett.* **18**, 1053 (1993).
- [53] R. Paschotta, K. Fiedler, P. Kurz, and J. Mlynek, *Appl. Phys. Lett.* **58**, 117 (1994).
- [54] V. Berger, *J. Opt. Soc. Am. B* **14**, 1351 (1997).
- [55] I. I. Zootoverkh, K. N. V., and E. G. Lariontsev, *Quantum Electronics* **30**, 565 (2000).
- [56] B. Maes, P. Bienstman, and R. Baets, *J. Opt. Soc. Am. B* **22**, 1378 (2005).
- [57] M. Liscidini and L. A. Andreani, *Phys. Rev. E* **73**, 016613 (2006).
- [58] S. Schiller, Ph.D. thesis, Stanford University, Stanford, CA (1993).
- [59] A. Ashkin, G. D. Boyd, and J. M. Dziedzic, *IEEE J. Quantum Electron.* **2**, 109 (1966).
- [60] I. B. Burgess, A. W. Rodriguez, M. W. McCutcheon, J. Bravo-Abad, Y. Zhang, S. G. Johnson, and M. Loncar, *OE* **17**, 9241 (2009).
- [61] M. W. McCutcheon, D. E. Chang, Y. Zhang, M. D. Lukin, and M. Loncar, *arXiv:0903.4706* (2010).
- [62] Y. H. Avetisyan, *Proc. SPIE* **3795**, 501 (1999).
- [63] R. A. Baumgartner and R. L. Byer, *IEEE J. Quantum Electron.* **15**, 432 (1979).
- [64] A. Yariv, *Quantum Electronics, 3rd ed.* (Wiley, New York, 1998).
- [65] G. T. Moore, K. Koch, and E. C. Cheung, *Optics Communications* **113**, 463 (1995).
- [66] M. Liscidini and L. A. Andreani, *Appl. Phys. Lett.* **85**, 1883 (2004).
- [67] Y. Dumeige and P. Feron, *Phys. Rev. A* **74**, 063804 (2006).
- [68] S. Stivala, A. C. Busacca, A. Pasquazi, R. L. Oliveri, R. Morandotti, and G. Assanto, *OL* **35**, 363 (2010).

- [69] A. I. Ferguson and M. H. Dunn, *IEEE J. Quantum Electron.* **13**, 751 (1977).
- [70] M. Brieger, H. Busener, A. Hese, F. V. Moers, and A. Renn, *Opt. Commun.* **38**, 423 (1981).
- [71] J. C. Bergquist, H. Hemmati, and W. M. Itano, *Opt. Commun.* **43**, 437 (1982).
- [72] W. J. Kozlovsky, W. P. Risk, W. Lenth, B. G. Kim, G. L. Bona, H. Jaeckel, and D. J. Webb, *Appl. Phys. Lett.* **65**, 525 (1994).
- [73] G. J. Dixon, C. E. Tanner, and C. E. Wieman, *Opt. Lett.* **14**, 731 (1989).
- [74] M. J. Collet and R. B. Levien, *Phys. Rev. A* **43**, 5068 (1991).
- [75] M. A. Persaud, J. M. Tolchard, and A. I. Ferguson, *IEEE J. Quantum Electron.* **26**, 1253 (1990).
- [76] K. Schneider, S. Schiller, and J. Mlynek, *Opt. Lett.* **21**, 1999 (1996).
- [77] X. Mu, Y. J. Ding, H. Yang, and G. J. Salamo, *Appl. Phys. Lett.* **79**, 569 (2001).
- [78] G. McConnell, A. I. Ferguson, and N. Langford, *J. Phys. D: Appl. Phys.* **34**, 2408 (2001).
- [79] T. V. Dolgova, A. I. Maidykovski, M. G. Martemyanov, A. A. Fedyanin, O. A. Aktsipetrov, G. Marowsky, V. A. Yakovlev, G. Mattei, N. Ohta, and S. Nakabayashi, *J. Opt. Soc. Am. B* **19**, 2129 (2002).
- [80] T.-M. Liu, C.-T. Yu, and C.-K. Sun, *Appl. Phys. Lett.* **86**, 061112 (2005).
- [81] L. Scaccabarozzi, M. M. Fejer, Y. Huo, S. Fan, X. Yu, and J. S. Harris, *OL* **31**, 3626 (2006).
- [82] C. M. Savage and D. F. Walls, *Optica Acta* **30**, 557 (1983).
- [83] E. Abraham, W. J. Firth, and J. Carr, *Physics Lett. A* pp. 47–51 (1982).
- [84] A. Siegman, *Lasers* (University Science Books, Mill Valley, CA, 1986).
- [85] M. D. Levenson, R. M. Shelby, A. Aspect, M. Reid, and D. F. Walls, *Phys. Rev. A* **32**, 1550 (1985).
- [86] N. Shibata, R. P. Braun, and R. G. Waarts, *IEEE J. Quantum Electron.* **QE-23**, 1205 (1987).
- [87] K. Inoue, *J. Lightwave Tech.* **10**, 1553 (1992).
- [88] M. Karisson, *JOSA-B* **15**, 2269 (1998).
- [89] J. Hansryd, P. A. Andrekson, M. Westlund, J. Li, and P. O. Hedekvist, *IEEE J. Quantum Electron.* **8**, 506 (2002).
- [90] L. Deng, E. W. Hagley, M. Trippenbach, Y. Band, P. S. Julienne, J. E. Simsarian, K. Helmerson, S. L. Rolston, and W. D. Phillips, *Nature* **398**, 218 (1999).
- [91] J. Feinberg, *Opt. Lett.* **7**, 486 (1982).
- [92] S. Watanabe, T. Naito, and T. Chikama, *PTL* **5**, 92 (1993).
- [93] G. P. Agrawal, *Fiber-Optic Communication Systems* (Wiley, Hoboken, NJ, 2002).
- [94] H. P. Yuen and J. H. Shapiro, *Opt. Lett.* **4**, 334 (1979).
- [95] R. E. Slusher, L. W. Hollberg, B. Yurke, J. C. Mertz, and J. F. Valley, *Phys. Rev. Lett.* **55**, 2409 (1985).
- [96] A. Pasquazi, Y. Park, J. A. na, F. Légaré, R. Morandotti, B. E. Little, S. T. Chu, and D. J. Moss, *Opt. Express* **18**, 7634 (2010).
- [97] A. Pasquazi, R. Ahmad, M. Rochette, M. Lamont, B. E. Little, S. T. Chu, R. Morandotti, and D. J. Moss, *Opt. Express* **18**, 3858 (2010).
- [98] G. Bartal, O. Manela, and M. Segev, *Phys. Rev. Lett.* **97**, 073906 (2006).
- [99] Y. C. Huang and Y. Y. Lin, *JOSA-B* **21**, 777 (2003).
- [100] M. Troccoli, A. Belyanin, F. Capasso, E. Cubukcu, D. L. Sivco, and A. Y. Cho, *Nature* **433**, 845 (2005).
- [101] S. Maas, *Nonlinear microwave and RF circuits* (Artech House, 2003).
- [102] A. Taflov and S. C. Hagness, *Computational Electrodynamics: The Finite-Difference Time-Domain Method* (Artech, Norwood, MA, 2000).
- [103] W. Suh, Z. Wang, and S. Fan, *IEEE J. Quantum Electron.* **40**, 1511 (2004).
- [104] J. A. Armstrong, N. Bloembergen, J. Ducuing, and P. S. Pershan, *Phys. Rev.* **127**, 1918 (1962).
- [105] S. K. Choi, R. D. Li, C. Kim, and P. Kumar, *JOSA-B* **14**, 1564 (1997).
- [106] J. D. Jackson, *Classical Electrodynamics* (Wiley, New York, 1998), 3rd ed.
- [107] M. L. Povinelli, M. Loncar, M. Ibanescu, E. J. Smythe, S. G. Johnson, F. Capasso, and J. D. Joannopoulos, *Opt. Lett.* **30**, 3042 (2005).
- [108] M. Tabor, *Chaos and Integrability in Nonlinear Dynamics: An Introduction* (Wiley, New York, 1989).